

## Original Article

# Adaptive Control of Network Frequency by Doubly-Fed Induction Generators Using a Data-Driven Method

Ebadollah Amouzad Mahdiraji<sup>1\*</sup> | Mojtaba Sedghi Amiri<sup>2</sup><sup>1</sup>Department of Engineering, Sari Branch, Islamic Azad University, Sari, Iran<sup>2</sup>Neka Power Generation Management Company, Iran**Citation** E.A. Mahdiraji, M.S. Amiri, **Adaptive Control of Network Frequency by Doubly-Fed Induction Generators Using a Data-Driven Method.** *Eurasian. J. Sci. Technol.* 2021, 1(2), 75-91. <https://doi.org/10.48309/ejst.2021.130260>**Article info:****Received:** 05 January 2021**Accepted:** 12 May 2021**Available Online:** 14 May 2021**ID:** JSTR-2104-1007**Checked for Plagiarism:** Yes**Language Checked:** Yes**Keywords:**

Data-driven control, Hessian matrix, Doubly-fed induction generator, Adaptive control.

**ABSTRACT**

Nowadays, to involve wind turbines in controlling the network frequency, drop and inertia control methods are usually used for variable speed wind turbines. Adjusting the benefits of droop and inertia control loops is very effective on the performance of wind turbines, but due to the variability of wind speed and network conditions, adjusting the control coefficients that produce the best response in all conditions is impossible. In this paper, a new method for the comparative regulation of the gain of the droplet control loops and the inertia of the doubly-fed induction generator (DFIG) is presented. Also, due to the relief of problems and shortcomings of wind turbine and network modeling, the use of a data-driven method, which operates only on the input and output of the system, has been proposed. In the new idea presented for faster control and prevention of sharp frequency droop, new equations have been calculated to update the coefficients of the control loops using the second fault derivative, which is used in the comparative adjustment of the gain of the droop and inertia control loops. In the proposed control method, the next instantaneous output is first estimated using KVNN and then the coefficients of the frequency control loops are adjusted adaptively using the Hessian matrix. The simulation results for a DFIG wind farm show the proper performance of an adaptive method based on data-driven control in increasing the minimum frequency and improving the network frequency in a permanent and transient state when a fault occurs.

**Introduction**

**A**mong the various wind turbine structures capable of operating at different speeds and constant frequencies, doubly-fed induction generators (DFIGs) are of particular importance and acceptance because DFIG operates at high and low synchronous speeds and power. The rated power of the converter is

20% -30% of the rated power of the generator, which reduces the cost and losses of the converter. The doubly-fed induction generator is also capable of absorbing and generating reactive power. The structure connected to the DFIG network for wind energy generation is shown in Figure 1. The stator winding of this generator is directly connected to the mains and its rotor winding is connected to the network through a frequency converter [1-8].

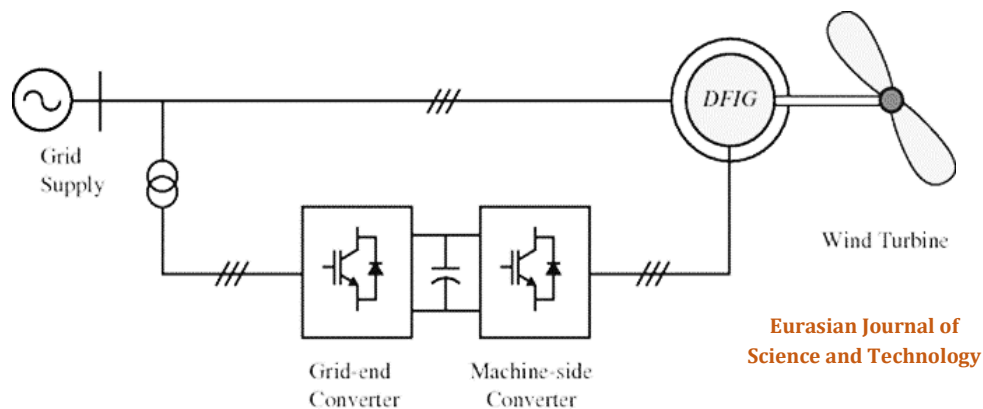


**Figure 1** DFIG diagram for wind power generation

One of the differences between wind turbines and synchronous generators in traditional power plants is that their active output power is independent of the grid frequency. Unlike synchronous generators, wind turbines do not have inherently stored energy to be released during frequency perturbations.

If the network power output and network power consumption are not equal, the network frequency changes according to the inertia of the system. As the penetration of wind turbines in the inertia network increases, power systems decrease and frequency fluctuations increase. For this reason, additional frequency control loops for wind turbines and wind farms have recently been proposed in laws and standards [9-14]. Inspired by traditional synchronous generators, some researchers have proposed a droop method for wind turbines. Droop control methods improve system frequency at a steady state [12].

On the basis a study [8], we proposed to participate in the initial response of the droop control frequency setting for distributed generation sources installed in the distribution network. In this method, the droop control is optimized according to the location and power of these sources by linearizing the load distribution equations, and the time-varying droop coefficient is proposed to prevent a sharp droop in wind turbine kinetic energy and to implement it at the highest possible power. Having focusing on wind turbines, many studies have suggested focusing on wind turbine inertia

energy during frequency perturbations to improve the frequency transient [21]. The power of wind turbine injection into the network is regulated by two different strategies with kinetic energy control [32]. In these methods, to control the network frequency, a sharp drop in wind turbine speed is prevented by adjusting the diagrams and the rate of frequency changes. Simultaneous use of droop and inertia control loops to improve the rate of frequency change and frequency droop has been expressed [33-36]. The combination of control loops increases the minimum network frequency during perturbation.

Increasing the gain of both control loops improves the lowest grid frequency during turbulence, but a large increase in these gains causes a drastic reduction in rotor speed. Given that the benefits of control loops are fixed numbers, adjusting them to their best value is very complicated and difficult at all wind speeds, during all network frequency disturbances. And with all the consuming loads leading to the best frequency response, it seems impossible. The combination of droop control and inertia control has been proposed to maintain the stability of the network and distributed generation units [1].

In this method, the changes of frequency angle and mains voltage and reduction of their fluctuations have been done by proportional distribution of active and reactive power between all sources. Also, the rate of change in the active output power of wind turbines has

recently been proposed as a limiting parameter of frequency control methods. A large increase in this rate causes wear and tear on wind generators and greatly increases maintenance costs. It is now proposed to limit the active power output rate of wind turbines to 0.2 (pu/s) [15].

It is worth noting that increasing the interest rate of the frequency control loops increases the rate. To design and adjust the control loops in the existing methods, presenting a good model of a wind turbine is a key point. When proposing wind turbine models, their proper performance in the following two times is very important: 1) Dynamic behavior of wind turbines during turbulence in power networks [46-48], and 2) dynamic behavior of wind turbines during wind changes [1].

For this reason, many articles have focused on providing a suitable model of a wind turbine to control the desired frequency, but it is very difficult to provide a suitable model to meet the above two goals that lead to the proper design of frequency control loops [5].

In general, there is a modeling problem in the controller design in all systems, therefore, the use of data-driven methods that design the controller without using the system model has been introduced [15]. But so far, data-driven methods have not been used to control network frequency. In view of the above considerations, an adaptive control method that has the ability

to adjust the coefficients of droop and inertia control loops in different wind and network conditions without the need for system modeling seems necessary, so this paper as a new method to adaptive control suggests droop control and inertia control loops using the data-driven method for DFIG. The data-driven method operates without the need for wind turbines and network models and only based on system input-output information.

This study addresses DFIG control in wind turbines in Section 2 and how to track active and reactive capacities from their reference values.

### *Control of Doubly-fed Induction Generators in Wind Turbines*

The stator of doubly-fed induction generators is connected directly to the mains and usually, its rotor is connected to the mains through two back-to-back converters. In most control methods, the network side converter is used to keep the DC link voltage constant and the main task of controlling and achieving the control goals is the rotor side converter. Control methods have been proposed for DFIG with different control objectives. In practice, DFIG power control methods are usually of particular importance since the inherent task of any generator is to inject active and reactive power into the grid.

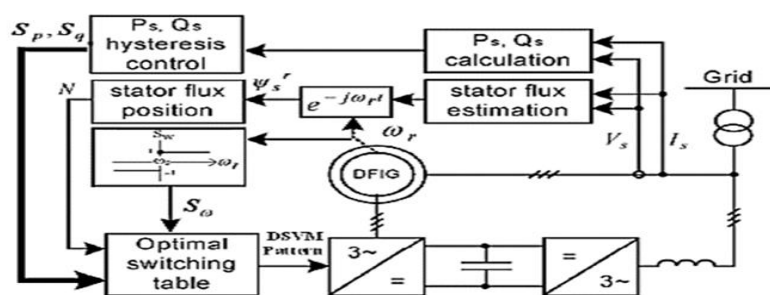


**Figure 2** Outline of direct power control

Details of the electrical model and direct power control method for DFIG are given [2]. The block diagram of this control method is shown in Figure 2. The purpose of direct power

control is the direct and independent control of active and reactive power and the sequence of powers from their reference values in different wind speed conditions. In direct power control

methods, it is not stated how to calculate the best reference for active and reactive power injected into the network. The best active and reactive power required by the network is not discussed. In practice, the most suitable reference for the active and reactive power of generators is usually the output of the frequency and voltage controllers of the network, respectively. In this inquiry, the DFIG active power reference is calculated from the frequency control loops.

### Frequency Control of Doubly-fed Induction Generators with Wind Turbines

The equation for power injection into the grid is expressed by DFIG in Formula 1.

$$(1) \\ P^* = P_{mppt} + K_{droop} (f_{grid} - f_{ref}) + K \left( \frac{df_{grid}}{dt} \right)$$

$P_{mppt}$  is the maximum power that can be extracted from a wind turbine in normal operation, which is usually obtained at a screw angle of zero. As shown in figure 3, any of the methods of Droop Control or Inertia Control or a combination thereof can be used. Droop control is based on the difference in network frequency from the reference frequency  $P_{droop} = f_{grid} - f_{ref}$  and inertia control is based on the rate of network frequency changes of rotor speed and frequency drop, and this method is completed and improved [23]. The calculation of the best diagrams and practical details for this Droop controller adaptive adjustment in different generators and networks is not stated.

### Data-driven Control Method

Data-driven controller (DDC) is a control theory and method that uses only the input or output data online or offline of the system and uses the mathematical model without directly or indirectly using the information obtained. The convergence and robustness of this controller are guaranteed by accurate analysis and under logical assumptions. In many process controls programs, system descriptor functions are out of reach due to insufficient process information and complex system dynamics.

In the data-driven control method, accurate information of the process and no identification system is required and only the input and output of the controller system are measured. This means that a general controller can be used independently to control a particular class of industrial processes, so it is not necessary to design a specific controller for each process. Other advantages of the data-driven controller include no need for complex manual adjustment of control parameters, no need for the experimental signal of the learning process, being cheaper and faster controller than similar examples, simplicity, and ease of execution, low computational volume, high resistance to system process changes and ensures system convergence assuming limited system input and output. One of the appropriate, simple, and widely used methods of data-driven control is the lazy control method [10].

### Lazy Teaching Method

In the lazy training method, the value of the  $yq$  function is estimated at the  $\Phi q$  question point by focusing on its neighbors. This idea is based on storing the previous state of the system and then estimating the current output based on the neighbors of the current state.

Suppose from an unknown nonlinear system the mapping  $f: R^m \rightarrow R$  with  $N$  points

$$\Phi_i = [x_{i1}, x_{i1}, \dots, x_{im}]^T, \left\{ \left\{ \Phi_i, y_i \right\} \right\}_{i=1}^N$$

in progress.  $\Phi_i, y_i$  are the output and input at the  $i$  moment, respectively, and  $n, x_{in}$  are the input at the  $i$  moment.

First, points similar to the  $\Phi q$  question point are selected from the database. In this algorithm, the criterion of greater similarity, less distance between points and from the existing set of information  $K$ , the information vector in terms of distance is selected as follows.

$$(4) \\ \{(y(1), \phi(1)), (y(2), \phi(2)), \dots, (y(k), \phi(k))\} \\ D(\phi(1), \phi(t)) > D(\phi(2), \phi(t)) > \dots > D(\phi(k), \phi(t))$$

At different times the density of the information vectors  $\Phi(t)$  in the neighborhood of the query vector is not equal. Therefore, the number of appropriate information vectors to estimate the output of the current moment is unknown. For linear modeling of the system at the moment, the number of selected neighbors is variable, in other words,  $k_m, k_M$  where  $k \in [k_m, k_M]$  are the upper and lower limits of the number of neighbors, respectively. To calculate the linear model  $\hat{\beta}^{(k+1)}$  using neighbor  $k + 1$ , we directly use  $\hat{\beta}_k$  obtained from neighbor  $k$ . In general, the system model is calculated as follows:

$$(5) \begin{cases} v(k+1) = v(k) - \frac{v(k)\phi_{k+1}D_{k+1}\phi_{k+1}^T v(k)}{1 + D_{k+1}\phi_{k+1}^T v(k)\phi_{k+1}} \\ \gamma(k+1) = v(k+1)\phi_{k+1}D_{k+1} \\ e(k+1) = y_{k+1} - \phi_{k+1}^T \hat{\beta}(k) \\ \hat{\beta}(k+1) = \hat{\beta}(k) + \gamma(k+1)e(k+1) \end{cases}$$

The above recursive method is based on the idea of least squares fault.

$$(6) \quad e_i^{loo}(k+1) = \frac{y_i - \phi_i^T \hat{\beta}(k+1)}{1 - \phi_i^T v(k+1)\phi_i}$$

$e_i^{loo}(k+1)$  is estimation fault considering  $k$  neighbors, between  $y_i$  and the estimated output value by subtracting the  $i$ -th sample from the selected neighborhoods from the database. The proposed recursive model of Formula 6 calculates all the parameters necessary to calculate the Leave-one-out faults.

$e_i^{loo}(k+1)$  contains the fault in the linear model generated by  $k$  to one of the nearest neighboring question point vectors. The  $MSE^{loo}(K+1)$  parameter ( $K + 1$ ), which is the validity of the mean squares of the Leave-one-out fault, is calculated by Equation 7.

$$(7) \quad MSE^{loo}(k+1) = \frac{\sum_{i=1}^{k+1} D_i (e_i^{loo}(k+1))^2}{(\sum_{i=1}^{k+1} D_i)}$$

Using the winner takes all method, we select the best model to predict. The recalculation estimation process ends if:

(8)

$$MSE^{loo}(k+1) > MSE^{loo}(k), k+1 \in [k_{min}, k_{max}]$$

When equation 8 is established, the model  $\hat{\beta}(k+1)$  is a more inadequate estimate than the model  $\hat{\beta}(k)$ , in which case the return procedure ends with the selection of the neighbor  $k$ ; otherwise,  $k, k_{max}$  the neighbor is selected to model the question point.

Based on the modeling procedure described in the above relations, the number of  $k \in k_{min}, k_{max}$  neighbors to calculate the linear model  $\hat{\beta}$  and the estimate  $\hat{y}_k$  is obtained by examining  $MSE^{loo}(k+1)$ . This evaluation procedure results in the best linear regression based on information vectors, which creates the best local linear model in the current situation. The important point in the KVNN algorithm is to update the database. The  $\Phi_q$  information vector for which the current system output is estimated can be added to the database. For this point, the density  $\{D_i\}_{i=1}^{k_{max}}$  of the information vectors around the vector  $\Phi_q$  is decisive. The database update strategy is as follows.

1. If  $D_1 = 1$ , it means that there is an information vector equal to the  $\Phi_q$  vector in the database.
2. If  $D_1 < 1, D_\rho < \delta (\rho < k_{max})$ , it means that the density of information around  $\Phi_q$  is sufficient and as a result, this vector is not added to the database.
3. Otherwise,  $\Phi_q$  is added to the database.

### Introducing a New Method to Update the Droop and Inertia Controller Coefficients

Fault cost optimization patterns that are repetitive start with an initial condition and then improve in each step with the following relation.

$$(9) \quad \Delta x(k) = x(k+1) - x(k) = \eta(k)p(k)$$

Where  $p(k)$  is the search vector and  $\eta(k)$  is the training rate in step  $k$ . In the descending gradient method, the value of the search direction vector is equal to the negative of the cost function derivative and we have:

$$(10) \quad x(k + 1) = x(k) - \eta(k)g(k)$$

The vector  $g(k)$  is a derivative of the fault cost function relative to the parameter  $x(k)$  since the optimization parameters are PD controller coefficients.

$$(11) \quad g = \begin{bmatrix} \frac{\partial J}{\partial k_p} \\ \frac{\partial J}{\partial k_d} \end{bmatrix}, J(k) = \frac{1}{2}e(k)^2, e(k) = y_r(k) - y(k)$$

$$(12) \quad \begin{aligned} K_p(k) &= K_p(k - 1) + \Delta K_p \\ K_d(k) &= K_d(k - 1) + \Delta K_d \end{aligned}$$

$$(13) \quad u(k) = u(k - 1) + K_p(k)x_{c1} + K_d(k)x_{c2}$$

$$x_{c1} = e(k) - e(k - 1), x_{c2} = e(k) + e(k - 2) - 2 \cdot e(k - 1)$$

$$(14) \quad \begin{cases} \Delta K_p = -\eta \frac{\partial J}{\partial K_p} = -\eta \frac{\partial J}{\partial y} \cdot \frac{\partial y}{\partial u} \cdot \frac{\partial u}{\partial k_p} = -\eta e(k) \frac{\partial y}{\partial u} x_{c1} \\ \Delta K_d = -\eta \frac{\partial J}{\partial K_d} = -\eta \frac{\partial J}{\partial y} \cdot \frac{\partial y}{\partial u} \cdot \frac{\partial u}{\partial k_d} = -\eta e(k) \frac{\partial y}{\partial u} x_{c2} \end{cases}$$

Since these learning algorithms use only the first derivative, they have difficulty in setting coefficients due to repetitions, especially in adaptive and timely applications. Therefore, in this paper, the use of high-order optimization methods is suggested. In the first-order optimization, the function is approximated only by Taylor expansion linear expressions, while in the second-order optimization the second-order Taylor expansion non-linear expressions, which also include second-order derivatives, are used. In other words, this study suggests that the performance of the control system should be different in the following two cases:

1) When the fault increases and the rate of increase of the fault increases every moment

compared with the previous moment (the second derivative of the fault is positive).

2) When the fault increases and the rate of increase of the fault decreases every moment compared with the previous moment (the second derivative of the fault is negative).

In case 1, the situation is more critical and the control system has not been able to function properly so far and the fault is increasing sharply, so the control system needs a more drastic change, but in the second case, however, the error increases (derivative the first is a positive fault). However, the control system has been able to prevent the incremental fault rate and has acted somewhat appropriately, and probably by continuing the existing control method (if the improvement is not so slow that the system becomes unstable) the growth rate of the fault change is zero. The same analysis can be done inversely or the case where the fault rate change is negative.

Taylor's expansion to find the value of the function around a known point is as follows:

$$(15) \quad \begin{aligned} J(x(k + 1)) &= J(x(k)) + \Delta x(k) \nabla J(x(k)) \\ &+ \frac{1}{2} \Delta x(k) \nabla^2 J(x(k)) \Delta x^T(k) + \dots \end{aligned}$$

$$\nabla^2 J(x) = \begin{bmatrix} \frac{\partial^2 J}{\partial k_p \partial k_p} & \frac{\partial^2 J}{\partial k_p \partial k_d} \\ \frac{\partial^2 J}{\partial k_d \partial k_p} & \frac{\partial^2 J}{\partial k_d \partial k_d} \end{bmatrix}$$

Which  $\nabla^2 J(x)$  is called the Hessian matrix.

$$(16) \quad g(k) + H(k) \cdot x(k) = 0 \rightarrow x(k + 1) = x(k) - Hk^{-1}g(k)$$

Therefore, according to the learning rate:

$$(17) \quad \begin{bmatrix} k_p(k + 1) \\ k_d(k + 1) \end{bmatrix} = \begin{bmatrix} k_p(k) \\ k_d(k) \end{bmatrix} - \begin{bmatrix} \eta_p \\ \eta_d \end{bmatrix} \left\{ \begin{bmatrix} \frac{\partial^2 J}{\partial k_p \partial k_p} & \frac{\partial^2 J}{\partial k_p \partial k_d} \\ \frac{\partial^2 J}{\partial k_d \partial k_p} & \frac{\partial^2 J}{\partial k_d \partial k_d} \end{bmatrix}^{-1} \begin{bmatrix} \frac{\partial J}{\partial k_p} \\ \frac{\partial J}{\partial k_d} \end{bmatrix} \right\} e(k)$$

$$(18) \quad H^{-1} = \left[ \begin{array}{cc} \left(\frac{\partial y}{\partial u} x_{c1}\right)^2 & \left(\frac{\partial y}{\partial u}\right)^2 \cdot x_{c1} \cdot x_{c2} \\ \left(\frac{\partial y}{\partial u}\right)^2 \cdot x_{c1} \cdot x_{c2} & \left(\frac{\partial y}{\partial u} x_{c2}\right)^2 \end{array} \right]^{-1}$$

the singular condition, the expression  $\mu I$  is added.

We see that the Hessian matrix is not Positive Define, so to remove the Hessian matrix from

$$(19) \quad x(k + 1) = x(k) - (H(k) + \mu I)^{-1} g(k)$$

$$(20) \quad \begin{bmatrix} k_p(k + 1) \\ k_d(k + 1) \end{bmatrix} = \begin{bmatrix} k_p(k) \\ k_d(k) \end{bmatrix} - \begin{bmatrix} \eta_p \\ \eta_d \end{bmatrix} \left\{ \begin{bmatrix} \frac{\partial^2 J}{\partial k_p \partial k_p} & \frac{\partial^2 J}{\partial k_p \partial k_d} \\ \frac{\partial^2 J}{\partial k_d \partial k_p} & \frac{\partial^2 J}{\partial k_d \partial k_d} \end{bmatrix} + \begin{bmatrix} \mu & 0 \\ 0 & \mu \end{bmatrix} \right\}^{-1} \begin{bmatrix} \frac{\partial J}{\partial k_p} \\ \frac{\partial J}{\partial k_d} \end{bmatrix} e(k)$$

If  $\mu$  is too small, Equation 21 is very close to Equation 16, and if it is too large, Equation 21 is close to Equation 14.

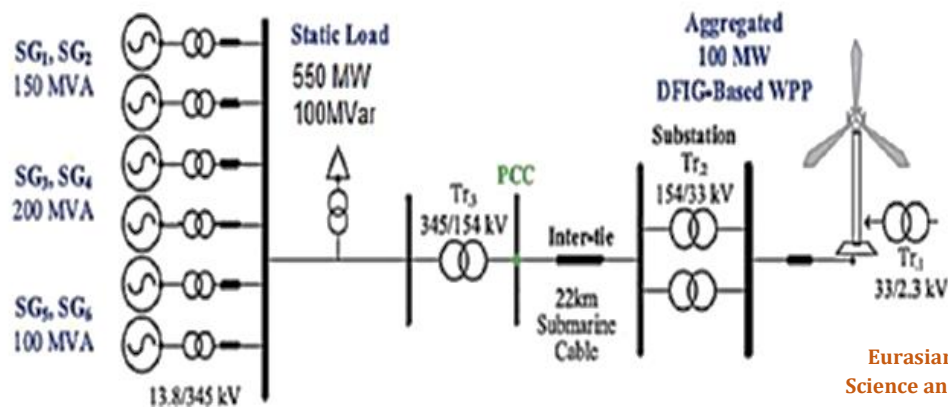
**Simulation**

Figure 4 shows the simulated system. As can be seen, the total number of generators connected to this network is 900 MV and its static load power is 550MW, 100MVar and the wind farm connected to the network with DFIG generators is equal to 100MW. In this simulation, a nominal frequency of 50Hz is considered.

Six synchronous generators include two 100MW generators, two 150MW generators and two 200MW generators connected to the grid. A 100MW gas plant [5], a 150MW hydroelectric plant [6] and other power plants are considered steam.

For all generators, 5% droop interest is considered and in Figure 5 and Table 1, the specifications of the steam turbine and its coefficients are stated and the specifications of the Guy and hydro power plants are stated in Annexes 1 and 2. The inertia constant is 4 for 100MW generators, 3 and 4 for 150MW generators and 5 for 200MW generators.

As for wind turbine generator, the wind turbine is modeled with a 100MW DFIG generator and is connected to the grid via a 2.3/33 kV transformer and then to the load and synchronous generators with a 22 km submarine cable with a voltage of 154 KV. Figure 6 shows the DFIG power curve and Figure 7 shows the limitations of electrical power and torque in this paper. In order to better and more accurately study the control methods and the effect of the benefits of the control loops, 4 different modes are simulated and analyzed.



**Figure 4** Study network

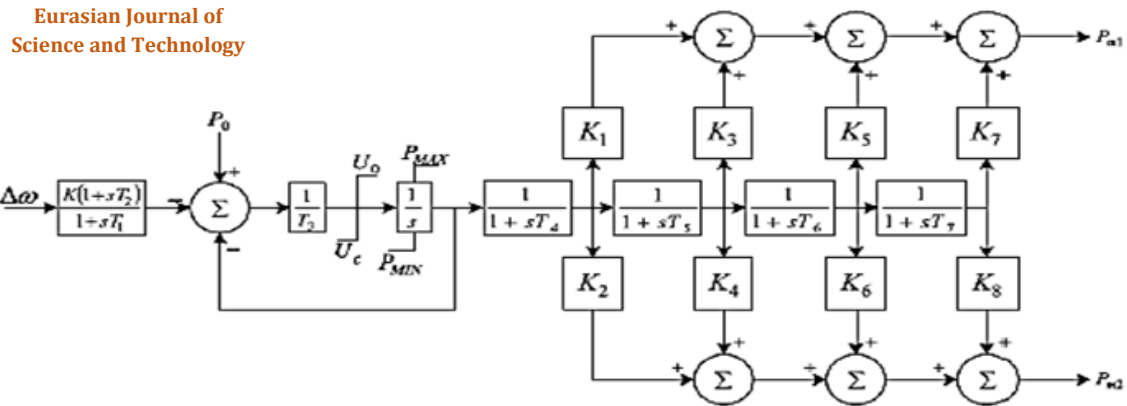


Figure 5 Governor model for IEEE G1 steam turbine

Table 1 Steam turbine governor parameters

K	K <sub>1</sub>	K <sub>2</sub>	K <sub>3</sub>	K <sub>4</sub>	K <sub>5</sub>	K <sub>6</sub>	K <sub>7</sub>	K <sub>8</sub>	P <sub>max</sub>
20	0.3	0	0.4	0	0.3	0	0	0	1
T <sub>1</sub>	T <sub>2</sub>	T <sub>3</sub>	T <sub>4</sub>	T <sub>5</sub>	T <sub>6</sub>	T <sub>7</sub>	U <sub>0</sub>	U <sub>c</sub>	P <sub>min</sub>
0.1	0	0.25	0.3	10	0.4	0	0.3	- 0.5	0.33

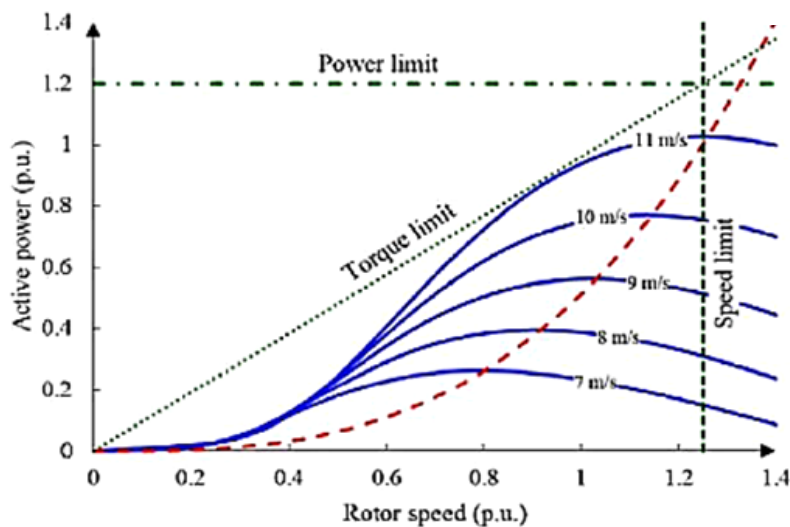
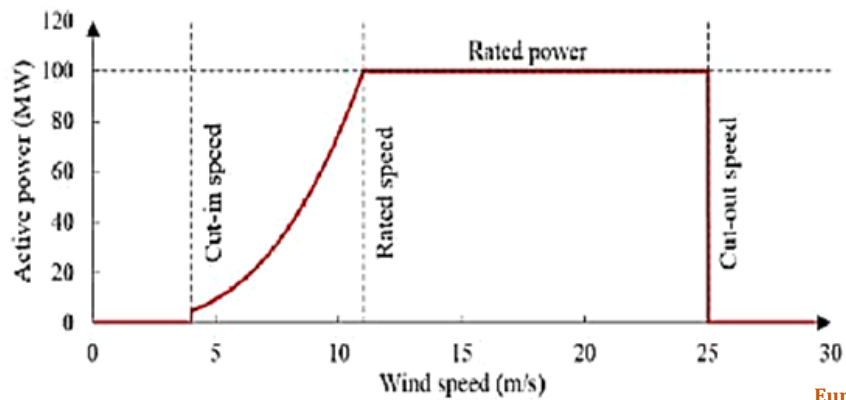
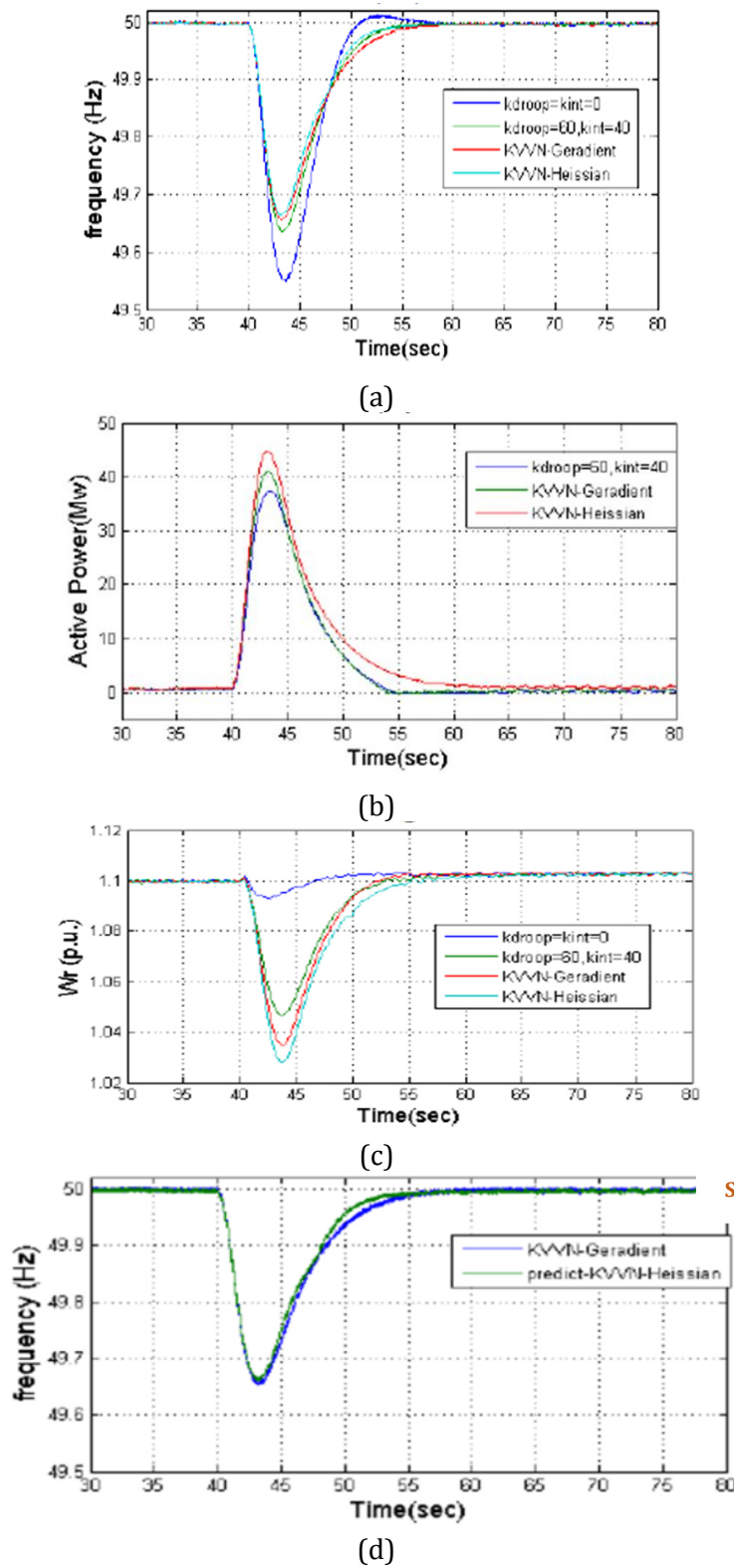


Figure 7 Active power and torque limits



**Figure 8** Network frequency results for mode 1 (a) Network frequency (b) Reference active power generated by the frequency control circuit (c) DFIG rotor speed (d) Frequency estimated by data-driven method

**Table 2** Comparison of network frequency for case 1

	$K_{\text{droop}}=0$	$K_{\text{droop}}=60$	KVNN	KVNN
	$K_{\text{inertia}}=0$	$K_{\text{inertia}}=40$	Gradient	Hessian
FN(Hz)	49.53	49.62	49.67	49.68
Max (ROCOF)	-0.490	-0.425	-0.335	-0.316

For better analysis of the proposed idea, 4 modes in each situation are simulated. In the first case, there is no frequency controller for the wind turbine. ( $K_{\text{droop}}=0$ ,  $K_{\text{int}}=0$ ), in the second case, both the droop and inertia controllers are present with a constant coefficient of  $K_{\text{droop}}=60$ ,  $K_{\text{int}}=40$  [2], in the third case of the KVNN controller by modifying the controller coefficients, the frequency is implemented using the descending gradient idea [3] and in the fourth case the KVNN controller is simulated by modifying the frequency controller coefficients using the Hessian matrix.

Case 1: Wind speed of 11m/s and 100MW thermal power plant out of the network.

In this case, the wind speed is 11m/s and generator 5 is disconnected from the mains at 40s when it generates 81MW of power. Figure 8 shows the system parameters in 4 modes. Figure 8- a shows the system frequency in different modes. The maximum value of ROCOF and the minimum value of frequency in the above cases are shown in Table 2. In the Hessian method, the velocity is greater because more power is released at the fault moment - which is why the grid frequency has the least velocity - but as it can be seen, it quickly returns to its original value.

At  $t = 54$ s, the speed, power, and frequency of all three return to the nominal value before the fault. That is, when the frequency returns to its nominal value, the additional power is injected by the frequency controller decreases and the speed approaches its nominal value. The active reference power generated by the wind turbine frequency and speed control circuit is shown in Figures 8-b and 8-c, respectively. The active reference power generated by the frequency

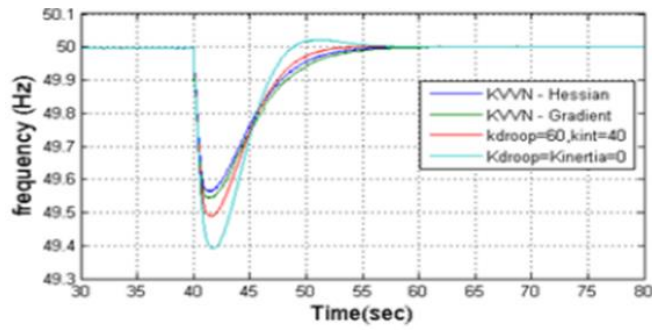
control circuit becomes zero when the network frequency is approximately equal to the reference frequency.

As stated, the main task of the data-driven method is to calculate the Jacobin matrix and estimate the frequency for the next step according to the information of previous times. The frequency estimated by the KVNN method and the actual frequency of the system are shown in Figure 8-D. As can be seen, the velocity estimation for both descending gradient and hessian methods is well done. In fact, the main reason for proper control for both methods is the correct estimation of the Jacobin matrix.

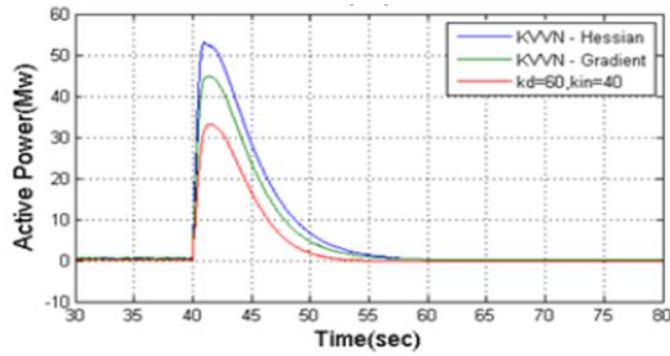
Case 2: Wind speed of 10m/s and 200MW thermal power plant out of the network.

In this case, the wind speed of 10m/s generates power and is disconnected from the network. In this case, a fault in wind speed occurs less than in case 1. Therefore, DFIG has less inertia to release power, but in this case, a fault occurs for a larger generator compared with in case 1, and the wind generator must inject more power into the network to maintain the frequency. Therefore, as we see in Figure 9, the frequency drop is greater in all 4 modes than that in the first mode [9].

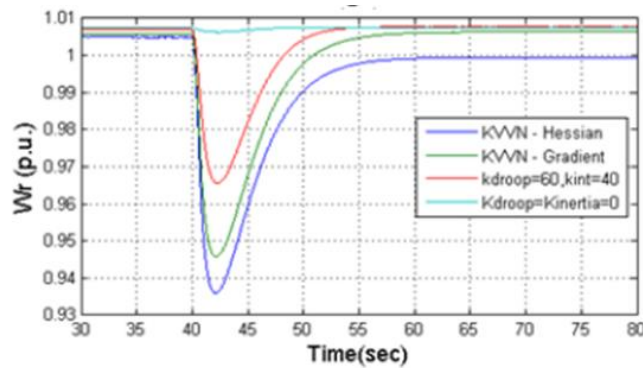
Figure 9- A shows the frequency of the system in different modes and the maximum value of ROCOF and frequency drop for frequency changes in 4 modes are shown in Table 3. The reference power calculated by the frequency controller is shown in Figure 9-b and the generator rotor speed is shown in Figure 9-d. As can be seen in Figure 9-c, the frequency estimation is well done, which indicates the correct operation of the data-driven control.



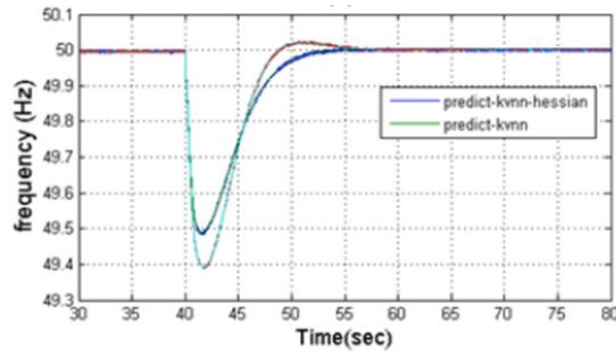
(a)



(b)



(c)



(d)

**Figure 9** Network frequency results for mode 2 (a) Network frequency (b) Reference active power generated by the frequency control circuit (c) DFIG rotor speed (d) Frequency estimated by data-driven method

**Table 3** Comparison of network frequency for case 2

	$K_{droop}=0$ $K_{inertia}=0$	$K_{droop}=60$ $K_{inertia}=40$	KVVN Gradient	KVVN Hessian
FN(Hz)	49.39	49.48	49.55	49.58
Max (ROCOF)	-0.740	-0.690	-0.640	-0.604

Case 3: When the wind speed is variable and the 200MW generator is disconnected from the main network [7].

In case of incorrect estimation of this matrix and as a result of incorrect estimation of the output frequency, the controller coefficients are not adjusted well [8].

In this section, to investigate the effect of continuous changes in wind speed on the performance of the control system, wind speed according to Figure 10 is considered as a variable [1].

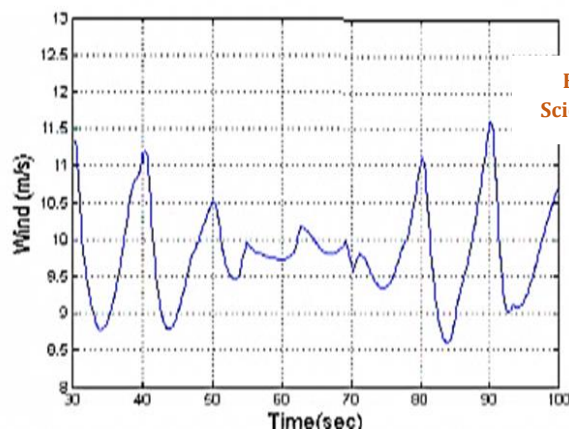
At  $t=40s$ , a 200MW synchronous generator injects 80MW of power into the grid and leaves the grid. Figure 11 shows the frequency changes for the 4 modes. As can be seen, the frequency droop is greater than in the previous case. Variable wind speed changes the rotor

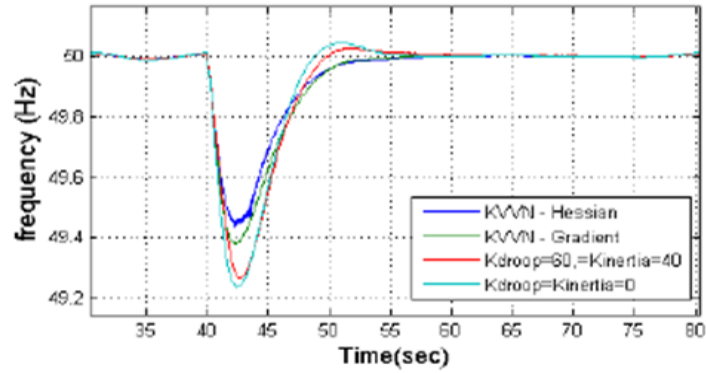
speed and thus changes the frequency. Figure 11- A shows the frequency of the system in different modes and the maximum value of ROCOF and frequency droop for frequency changes in 4 modes are shown in Table 4.

The reference power calculated by the frequency controllers and the generator rotor speed are shown in Figures 11-b and -11, respectively. The first step in the proper functioning of the proposed control method is the proper functioning of the data-driven control system. The main task of the data-driven method in the proposed control system is to correctly estimate the frequency and determine the Jacobin matrix coefficients. Figure 11- c shows the appropriate network frequency estimation for the two modes of the data-driven control method [5].

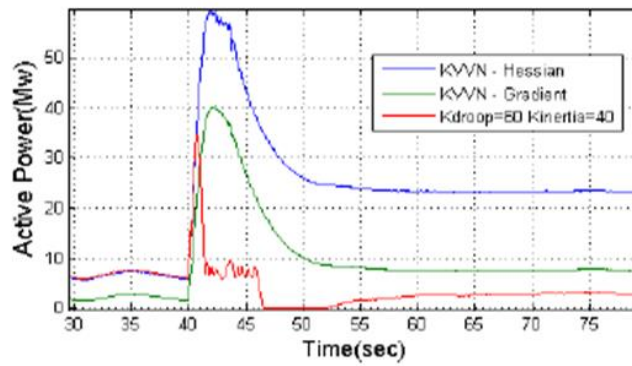
**Table 4** Comparison of network frequency for case 3

	$K_{droop}=0$ $K_{inertia}=0$	$K_{droop}=60$ $K_{inertia}=40$	KVVN Gradient	KVVN Hessian
FN(Hz)	49.21	49.24	49.39	49.42
Max (ROCOF)	-0.815	-0.782	-0.769	-0.722

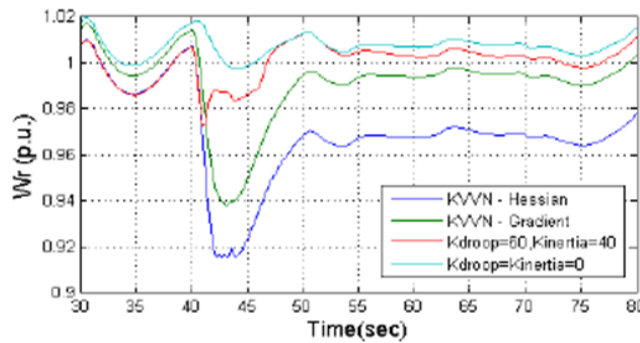
**Figure 10** Wind speed for case 3



(a)

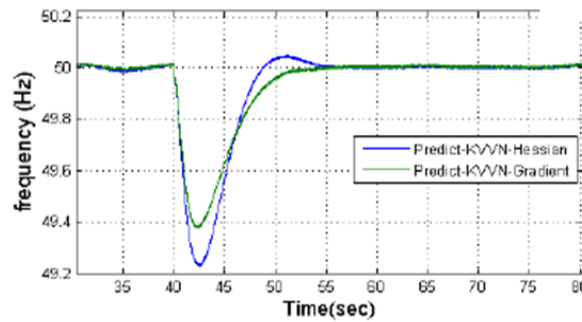


(b)



(c)

Eurasian Journal of Science and Technology



(d)

**Figure 11** Network frequency results for mode 3 (a) Network frequency (b) Reference active power generated by the frequency control circuit (c) DFIG rotor speed (d) Frequency estimated by data-driven method

A comparison of Figures 11 and 9 shows that the data-driven estimator functions well at constant speed and variable speed modes.

Case 4: The wind speed decrease and the 150MW thermal power plant out of the network.

In this section, to investigate the reduction of wind speed on the performance of the control system, the wind speed is considered according to Figure 12 and decreases from 11.5m/s to 9.7m/s between 40 to 50 seconds with a constant slope. At t=40s, a 150MW synchronous generator injects 89MW of power into the network and leaves the network. Figure 13 shows the frequency changes, active power, rotor speed and frequency prediction of the frequency control circuit for 4 cases, as in the previous sections. Figure 13-A shows the frequency of the system in different modes, and in Table 5, due to better and more accurate comparison, the minimum frequency and maximum value of ROCOF are expressed. Due to

the decrease in wind speed and kinetic energy of the wind turbine during the fault, the frequency droop is greater than that in all previous cases. Also, by comparing the four modes, it can be seen that the network frequency in its previous three modes of the network reaches its steady state in 56 seconds and in this mode in 63 seconds [7].

The reference power calculated by the frequency controller circuit is shown in Figure 13-b and the generator rotor speed is shown in Figure 13-D. As can be seen, due to the decrease in wind speed and the occurrence of faults, a severe decrease in rotor speed occurs and less kinetic energy is injected into the network during the fault compared with the previous cases. However, as shown in Figure 13-c, due to the proper estimation of the network frequency using data-driven methods, the proposed control method proves better than the other three modes.

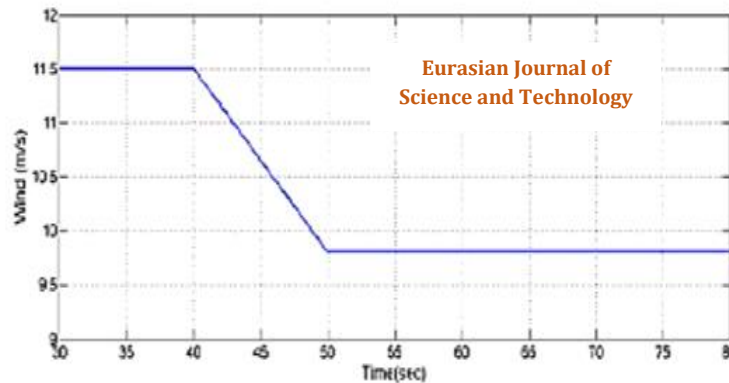
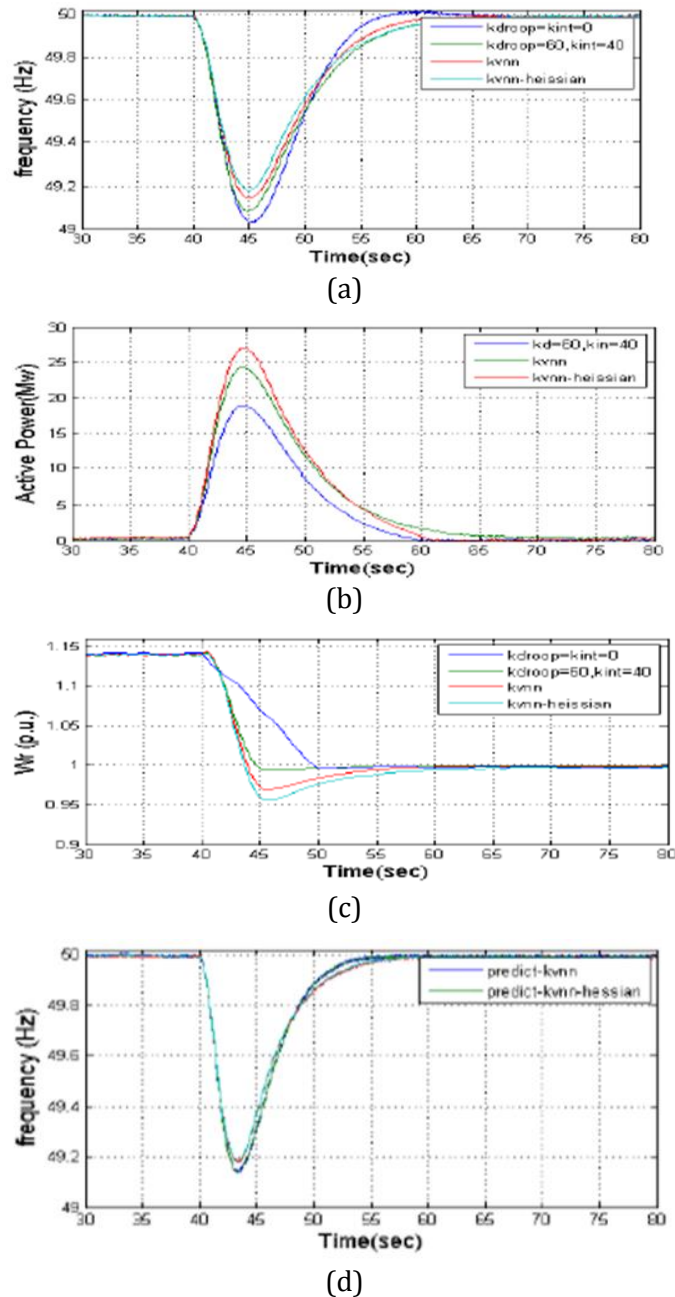


Figure 12 Wind speed for case 4

Table 5 Comparison of network frequency for mode 4

	$K_{droop}=0$	$K_{droop}=60$	KVVN	KVVN
	$K_{inertia}=0$	$K_{inertia}=40$	Gradient	Hessian
FN(Hz)	49.02	49.08	49.14	49.18
Max (ROCOF)	-0.841	-0.827	-0.802	-0.781



**Figure 13** Network frequency results for mode 4 (a) Network frequency (b) Reference active power generated by the frequency control circuit (c) DFIG rotor speed (d) Frequency estimated by data-driven method

### Conclusion

In this investigation, a new method is proposed for the comparative adjustment of the coefficients of Droop and DFIG control loops to improve the frequency of the power network. Also, to overcome the modeling problems, the data-driven method has been used, which operates only on the basis of system input and output. In this paper, the use of KVNN method

is proposed, which uses two parameters of size and angle between vectors to increase the speed and accuracy in finding similar neighbors.

Also, a new formulation is presented to update the coefficients of droop and inertia control loops using the Hessian fault matrix. One of the advantages of the proposed method is that it

can be used without the need for any initial analysis of wind turbines and power grids. Because the data-driven method uses only the network frequency information and the controller injection power. The KVNN method for adjusting the coefficients of the frequency control circuit using the instantaneous vectors predicts the network frequency for the next instant. Another important advantage of the proposed control system is the lower reduction of the network frequency due to the use of the Hessian matrix to adjust the coefficients of the frequency control circuit.

To investigate the effect of the proposed algorithm on wind turbine performance, we connected a 100MW DFIG wind farm with six synchronous generators with a total power of 900MW to a static load and simulated and compared the network performance in 4 different modes. The simulation results indicate the robustness and effectiveness of the control method presented in the transient and permanent state and the increase of the minimum value of the network frequency when the generators go out and the increase of the load in the constant and variable wind speed mode happens.

## ORCID

Ebadollah Amouzad Mahdiraji

<https://orcid.org/0000-0003-3777-4811>

## References

- [1] E.A. Mahdiraji, N. Ramezani, *International Academic Journal of Science and Engineering*, **2016**, *3*, 1-12. [[crossref](#)], [[Google Scholar](#)], [[Publisher](#)]
- [2] A. Bozorgian, S. Zarinabadi, A. Samimi, *Journal of Chemical Reviews*, **2020**, *2*, 122-129. [[crossref](#)], [[Google Scholar](#)], [[Publisher](#)]
- [3] E.A. Mahdiraji, M.S. Amiri, *Journal of Engineering in Industrial Research*, **2020**, *1*, 111-122. [[crossref](#)], [[Google Scholar](#)], [[Publisher](#)]
- [4] E.A. Mahdiraji, M.S. Amiri, *Journal of Engineering in Industrial Research*, **2021**, *2*, 7-16. [[crossref](#)], [[Google Scholar](#)], [[Publisher](#)]
- [5] E.A. Mahdiraji, N. Ramezani, *International Academic Journal of Science and Engineering*, **2016**, *3*, 1-12. [[crossref](#)], [[Google Scholar](#)], [[Publisher](#)]
- [6] E.A. Mahdiraji, *CRPASE: Transactions of Electrical, Electronic and Computer Engineering* **2020**, *6*, 245-250. [[crossref](#)], [[Google Scholar](#)], [[Publisher](#)]
- [7] E.A. Mahdiraji, *Journal of Scientific Perspectives*, **2020**, *4*, 245-254. [[crossref](#)], [[Google Scholar](#)], [[Publisher](#)]
- [8] E.A. Mahdiraji, S.M. Shariatmadar, *Advanced Journal of Science and Engineering*, **2020**, *1*, 27-31. [[crossref](#)], [[Google Scholar](#)], [[Publisher](#)]
- [9] E.A. Mahdiraji, A.Y. Talouki, *Journal of Chemical Reviews*, **2020**, *2*, 284-291. [[crossref](#)], [[Google Scholar](#)], [[Publisher](#)]
- [10] E.A. Mahdiraji, A.Y. Talouki, *Journal of Chemical Reviews*, **2021**, *3*, 40-49. [[crossref](#)], [[Google Scholar](#)], [[Publisher](#)]
- [11] F. Zare Kazemabadi, A. Heydarinasab, A. Akbarzadeh, M. Ardjmand, *Artificial cells, nanomedicine, and biotechnology*, **2019**, *47*, 3222-3230. [[crossref](#)], [[Google Scholar](#)], [[Publisher](#)]
- [12] F. Zare Kazemabadi, A. Heydarinasab, A. Akbarzadehkhiyavi, M. Ardjmand, *Chemical Methodologies*, **2021**, *5*, 135-152. [[crossref](#)], [[Google Scholar](#)], [[Publisher](#)]
- [13] S. M. S. Mirnezami, F. Zare Kazemabadi, A. Heydarinasab, *Progress in Chemical and Biochemical Research*, **2021**, *4*, 191-206. [[crossref](#)], [[Google Scholar](#)], [[Publisher](#)]
- [14] M.E. Bidhendi, Z. Asadi, A. Bozorgian, A. Shahhoseini, M.A. Gabris, *Environmental Progress & Sustainable Energy*, **2020**, *39*, 13306. [[crossref](#)], [[Google Scholar](#)], [[Publisher](#)]
- [15] M. Garmroodi, G. Verbic, D.J. Hill, *IEEE Transactions on Sustainable Energy*, **2018**, *9*, 676-684. [[crossref](#)], [[Google Scholar](#)], [[Publisher](#)]
- [16] A. Teninge, C. Jecu, D. Roye, S. Bacha, J. Duval, R. Belhomme, *IET Renew. Power Gener.*, **2009**, *3*, 358-370. [[crossref](#)], [[Google Scholar](#)], [[Publisher](#)]

- [17] A. Bozorgian, *Journal of Engineering in Industrial Research*, **2020**, *1*, 1-19. [[crossref](#)], [[Google Scholar](#)], [[Publisher](#)]
- [18] A. Mitra, D. Chatterjee, *IEEE Trans. Power Syst.*, **2016**, *31*, 82-93. [[crossref](#)], [[Google Scholar](#)], [[Publisher](#)]
- [19] A. Bozorgian, *Progress in Chemical and Biochemical Research*, **2020**, *3*, 169-179. [[crossref](#)], [[Google Scholar](#)], [[Publisher](#)]
- [20] N. Kayedi, A. Samimi, M. Asgari Bajgirani, A. Bozorgian, *South African Journal of Chemical Engineering*, **2021**, *35*, 153-158. [[crossref](#)], [[Google Scholar](#)], [[Publisher](#)]
- [9] E.A. Mahdiraji, *Journal of Chemical Reviews*, 2020; *3*, [[crossref](#)], [[Google Scholar](#)], [[Publisher](#)]
- [21] A. Bozorgian, S. Zarinabadi, A. Samimi, *Journal of Chemical Reviews*, **2020**, *2*, 122-129. [[crossref](#)], [[Google Scholar](#)], [[Publisher](#)]
- [22] S.E. Mousavi, A. Bozorgian, *International Journal of New Chemistry*, **2020**, *7*, 195-219. [[crossref](#)], [[Google Scholar](#)], [[Publisher](#)]
- [23] E. A. Mahdiraji, N. Ramezani, "Transient modeling of transmission lines components with respect to corona phenomenon and grounding system to reduce the transient voltages caused by lightning Impulse," 2015 2nd International Conference on Knowledge-Based Engineering and Innovation (KBEI), Tehran, Iran, **2015**, 405-411. [[crossref](#)], [[Google Scholar](#)], [[Publisher](#)]
- [24] A. Bozorgian, *Advanced Journal of Chemistry, Section B*, **2020**, *2*, 91-101. [[crossref](#)], [[Google Scholar](#)], [[Publisher](#)]